Received: 15 February 2017 | Accepted: 5 July 2017

DOI: 10.1002/hyp.11276

WILEY

RESEARCH ARTICLE

Development of a soil moisture-based distributed hydrologic model for determining hydrologically based critical source areas

Sisi Li[1,2,3] | Margaret Gitau[2] | David Bosch[4] | Bernard A. Engel[2] | Liang Zhang[1] | Yun Du[1]

[1] Key Laboratory for Environment and Disaster Monitoring and Evaluating, Institute of Geodesy and Geophysics, Chinese Academy of Sciences, Wuhan, China

[2] Department of Agricultural and Biological Engineering, Purdue University, West Lafayette, IN, USA

[3] University of Chinese Academy of Sciences, Beijing, China

[4] USDA-ARS Southeast Watershed Research Lab, Tifton, GA, USA

Correspondence
Liang Zhang, Key Laboratory for Environment and Disaster Monitoring and Evaluating, Institute of Geodesy and Geophysics, Chinese Academy of Sciences, 340 XuDong Road, Wuhan 430077, China.
Email: lzhang@whigg.ac.cn

Funding information
National Key Research and Development Program of China, Grant/Award Number: 2016YFD0800500; National Natural Science Foundation of China, Grant/Award Number: 41471433; Youth Innovation Promotion Association of the Chinese Academy of Sciences, Grant/Award Number: 2016304; China Scholarship Council, Grant/Award Number: 201504910561

Abstract

A simple grid cell-based distributed hydrologic model was developed to provide spatial information on hydrologic components for determining hydrologically based critical source areas. The model represents the critical process (soil moisture variation) to run-off generation accounting for both local and global water balance. In this way, it simulates both infiltration excess run-off and saturation excess run-off. The model was tested by multisite and multivariable evaluation on the 50-km^2 Little River Experimental Watershed I in Georgia, U.S. and 2 smaller nested subwatersheds. Water balance, hydrograph, and soil moisture were simulated and compared to observed data. For streamflow calibration, the daily Nash-Sutcliffe coefficient was 0.78 at the watershed outlet and 0.56 and 0.75 at the 2 nested subwatersheds. For the validation period, the Nash-Sutcliffe coefficients were 0.79 at the watershed outlet and 0.85 and 0.83 at the 2 subwatersheds. The per cent bias was less than 15% for all sites. For soil moisture, the model also predicted the rising and declining trends at 4 of the 5 measurement sites. The spatial distribution of surface run-off simulated by the model was mainly controlled by local characteristics (precipitation, soil properties, and land cover) on dry days and by global watershed characteristics (relative position within the watershed and hydrologic connectivity) on wet days when saturation excess run-off was simulated. The spatial details of run-off generation and travel time along flow paths provided by the model are helpful for watershed managers to further identify critical source areas of non-point source pollution and develop best management practices.

KEYWORDS

infiltration excess run-off, non-point source pollution, saturation excess run-off, soil moisture, soil topographic index, spatially distributed model

1 | INTRODUCTION

Management practices generally need to be adjusted on a location basis, given the integral role that site and watershed hydrology plays on nutrient (and sediment) transfers (Kleinman et al., 2011). Precise and cost-effective watershed management requires spatial details of hydrologic characteristics, such as run-off generation areas. Run-off generation areas together with nutrient source areas can be used to identify critical source areas (CSAs; Pionke, Gburek, Sharpley, & Schnabel, 1996), which help managers concentrate their resources on the riskiest areas of a watershed. Models are usually regarded by researchers as efficient tools for determining CSAs and developing best management practices. However, there are limited applications of currently common watershed models (such as Soil and Water Assessment Tool or SWAT (Arnold, Srinivasan, Muttiah, & Williams, 1998), Hydrological Simulation Program–Fortran (Becknell, Imhoff, Kittle, Donigian, & Johanson, 1993), etc.) by conservation managers for delineating CSAs and for implementing measures to control non-point source pollution. The relatively infrequent application of these models may be mainly due to their complexity and parameter intensity that require advanced skills to use them. Also, the infrequent application can be attributed to their generation of simulation results on naturally occurring hydrologic scales (usually subwatershed), which are relatively coarse for management practices usually meaningful at the farm-scale (Ghebremichael, Veith, & Hamlett, 2013). This has motivated developers of SWAT to introduce a restructured version, SWAT+ (Bieger et al., 2017) that has landscape units (spatially referenced simulation levels) within subwatersheds, as well as a grid-cell-

based SWAT landscape model (Rathjens, Oppelt, Bosch, Arnold, & Volk, 2015).

Determining hydrologically based CSAs for precise and cost-effective management does not only require simpler hydrologic models having finer spatial resolution; more importantly, hydrologic models should reasonably represent run-off generation mechanisms since they largely control run-off generation areas (Lyon, McHale, Walter, & Steenhuis, 2006). In the infiltration excess run-off theory, run-off is generated where local precipitation rate is greater than local infiltration rate. It appears scattered across a watershed determined by site precipitation, land cover, soil properties, and soil moisture condition, most of which are local characteristics. By contrast, saturation excess run-off is generated where precipitation exceeds the soil moisture capacity, usually in lowland areas within a watershed that are hydrologically connected to water bodies. In this sense, watershed global characteristics are the main governing factors of saturation run-off generation areas. However, there is a gap between the run-off generation mechanism used in operational models and those observed by experimentalists. Many operational hydrologic models exclusively represent one specific overland run-off, for example: infiltration excess run-off by AnnAGNPS (Bingner & Theurer, 2001), GWLF (Haith & Shoemaker, 1987), and Hydrological Simulation Program–Fortran; or saturation excess run-off by TOPMODEL (Beven, 1995) and Soil Moisture Routing model (Frankenberger, Brooks, Walter, Walter, & Steenhuis, 1999). However, field observations have detected both overland run-off and subsurface stormflow in the same watershed or even same hillslope from semi-arid to subhumid regions (Calvo-Cases, Boix-Fayos, & Imeson, 2003; Martinez-Mena, Albaladejo, & Castillo, 1998; Saffarpour, Western, Adams, & McDonnell, 2016; Srinivasan, Gburek, & Hamlett, 2002; Srinivasan & McDowell, 2009). There are recent attempts to incorporate different run-off generation mechanisms in one model (Boll, Brooks, Crabtree, Dun, & Steenhuis, 2015; Guo, Liu, & Baetz, 2012; Li, Sivapalan, & Tian, 2012). Still, it is challenging and worthwhile to seek a simpler method that reasonably represents different run-off generation mechanisms.

The solution to representing both run-off generation mechanisms probably lies in the representation of antecedent soil moisture. Pre-event water largely dominates storm run-off (Kirchner, 2003), and soil moisture is observed to impact the threshold of run-off generation (Penna, Tromp-van Meerveld, Gobbi, Borga, & Dalla Fontana, 2011). Soil moisture update in infiltration excess run-off models is usually based on water balance accounting for local water input (infiltration) and output (evapotranspiration, percolation; Mishra & Singh, 2004; Soulis & Dercas, 2007; Soulis & Dercas, 2010). By contrast, subsurface lateral water movement significantly impacts the spatial distribution of soil moisture in saturation excess run-off theory (Dunne & Black, 1970). Soil topographic index (STI), a global watershed characteristic related to relative position and hydrologic connectivity, is usually used to account for subsurface water movement impact (Lyon, Walter, Gérard-Marchant, & Steenhuis, 2004). Hence, to represent both run-off mechanisms, soil moisture variation should be simulated accounting for both local and global water balance.

In this study, a simple grid-cell-based distributed hydrologic model for watershed management (DHM-WM) was developed to simulate reasonable spatial variations of run-off generation and to determine hydrologically based CSAs. To meet the goal, the model represents both infiltration excess and saturation excess run-off through distributed estimation of soil moisture variation accounting for both local and global water balance. The DHM-WM was applied in a small watershed to test its ability to estimate soil moisture and streamflow variations as well as its ability to simulate distributed run-off under both infiltration excess and saturation excess mechanisms.

2 | METHODS

2.1 | General model concepts and structures

DHM-WM was developed to simulate daily soil moisture, surface run-off, subsurface stormflow, and base flow on a grid cell basis. Soil moisture is updated on a daily time step accounting for both local and global water balance. The distributed soil moisture is used as the antecedent moisture condition to simulate daily infiltration excess run-off based on the long-term curve number (CN) method developed by Mishra and Singh (2004), referred to as the Mishra-Singh CN method later in this paper. Saturation excess run-off and subsurface stormflow are simulated if the subsurface water table exceeds a threshold according to the global water balance. Saturation excess run-off and infiltration excess run-off are added together on a grid cell basis and routed to calculate surface flow to water bodies. Base flow is also simulated using a module based on the Mishra-Singh CN method. Streamflow to water bodies is the sum of surface flow, subsurface stormflow, and base flow and is reported on each simulation day.

To simulate soil moisture variation, the soil profile is approximated as two layers (the upper unsaturated and the lower saturated layers), and its water exchange with water bodies is accounted for, as illustrated in Figure 1. The unsaturated layer is defined by the water table as the lower bound and the soil surface as the upper bound. The total amount of soil moisture in the unsaturated layer (M) is updated daily accounting for local water balance with infiltration (F_d) as input, and evapotranspiration (ET_{upper}) and downward percolation as output. The saturated layer is defined by the water table as the upper bound and the restrictive layer as the lower bound, and the soil moisture content is M_{bal}. Besides getting percolation water from the upper layer and losing water with evapotranspiration (ET_{lower}), this layer also has lateral subsurface water movement across the watershed. Subsurface water movement results in variation of water table depth as well as water exchange between landscape soils and water bodies.

To make the model structure simpler yet still able to provide spatially and temporally realistic simulations, DHM-WM takes advantage of two modifications of the Mishra-Singh CN method. One is separating infiltration into gravitational infiltration (Fc), the rate of which is constant, and dynamic infiltration (Fd), the rate of which decreases as soils get wetter during a rainfall event. Gravitational infiltration recharges the ground water aquifer and is used to calculate base flow with a simple routing equation. In the second modification, antecedent soil moisture (M) is explicitly included in the equation of run-off estimation, which avoids incorporating extra parameters to establish the relationship between soil moisture and the retention coefficient (S) in the traditional CN method. It should be noted that

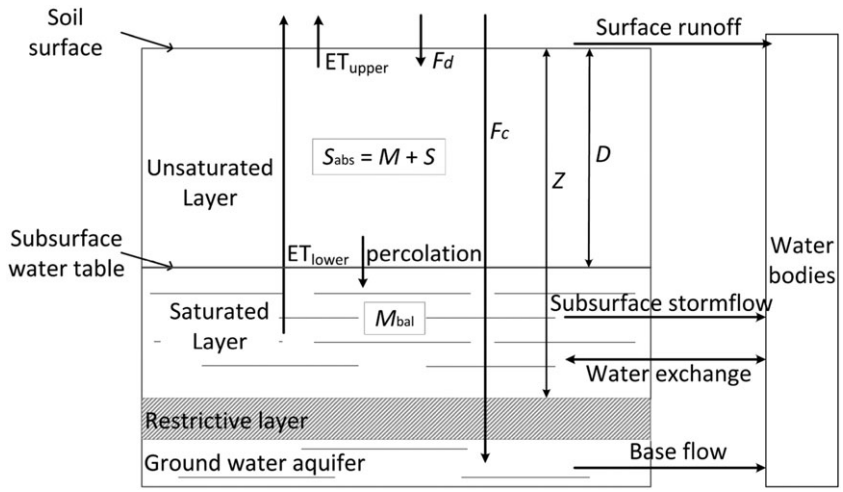

FIGURE 1 Two-layer approximation of soil profile and main processes in distributed hydrologic model for watershed management

Fc is assumed to go through the soil profile, so it is excluded from the water balance for soil moisture update in DHM-WM. In addition, the sum of *M* and *S* equals S_{abs}, the absolute retention coefficient in the Mishra-Singh CN method. In DHM-WM which represents spatially and temporally variable water table depth, S_{abs} is heterogeneous and dynamic and calculated as $S_{abs} = S_{abs\_mx} - M_{bal}$, where S_{abs_mx} is the maximum value of the absolute retention parameter or the S_{abs} in the very dry condition. The default value of S_{abs_mx} is associated with CN determined by soil–land cover combinations. It is then calibrated by multiplying an adjustment factor while maintaining the relative relationships among different soil–land cover combinations.

2.2 | Daily soil moisture update accounting for local and global water balance

2.2.1 | The upper unsaturated layer: local water balance

The soil moisture content (*M*) for the upper layer is updated daily accounting for local water input and output. It is first updated by adding *Fd* and extracting evapotranspiration from the unsaturated layer (ET_{upper}) during the daily time step as below:

$$M'_{i,t} = M_{i,t} + Fd_{i,(t,t+1)} - ET_{upper,i,(t,t+1)}, \quad (1)$$

where $M'_{i,t}$ and $M_{i,t}$ are the soil moisture of upper layer in grid cell *i* on day *t* after and before update, respectively. If $M'_{i,t}$ is higher than the field capacity of the soil (FC_i), then, the extra water moves by percolation and is represented as an exponential decline similar to SWAT model representation (Neitsch, Arnold, Kiniry, Williams, & King, 2011). Hence, moisture content in the unsaturated layer is updated again as below:

$$\begin{aligned} M_{i,t+1}/S_{abs,i,t} &= FC_i + \left(M'_{i,t}/S_{abs,i,t} - FC_i\right)\cdot \exp(-24/tM_i), && \text{if } M'_{i,t}/S_{abs,i,t} > FC_i, \\ M_{i,t+1}/S_{abs,i,t} &= M'_{i,t}/S_{abs,i,t}, && \text{if } M'_{i,t}/S_{abs,i,t} \le FC_i, \end{aligned} \quad (2)$$

where $M_{i,t+1}$ is the soil moisture of upper layer in grid cell *i* on day $t + 1$; tM_i is the time to drain in grid cell *i* in h, which determines the rate at which extra water goes from the unsaturated layer to the saturated layer. Because of lateral water movement, soil water tends to accumulate in lowland areas; thus, the headwater area should drain more quickly than the lowland area. Here, tM_i is assumed to be linearly related to STI of the grid cell as $tM_i = \overline{tM}\cdot STI_i/\overline{STI}$, where $\overline{tM}$ and $\overline{STI}$ are the average time to drain and average STI of the watershed, respectively. $\overline{tM}$ is a parameter that needs calibration.

Mishra and Singh (2004) calculate ET as potential ET (PET) multiplied by a soil water availability factor: $ET = PET \cdot (1 - (S/S_{abs})^2)$. Expanding on this method, DHM-WM calculates ET by further considering the effect of soil properties, that is, soils containing more clay have lower ET. Hence, The ET_{upper} in Equation 1 is calculated as

$$ET_{upper,i,(t,t+1)} = PET\cdot\left(1-\left(\frac{S_{i,t}}{S_{abs,i,t}}\cdot\frac{FC_i}{\overline{FC}}\right)^2\right), \quad (3)$$

where $\overline{FC}$ is the watershed average field capacity.

2.2.2 | The lower saturated layer: global water balance

For the lower saturated layer, transpiration is accounted for if the water table depth reaches the root zone as below:

$$\begin{aligned} ET_{soil,i,(t,t+1)} &= PET\cdot\left(1-\left(\frac{S_{i,t}}{S_{abs,RT,i,t}}\cdot\frac{FC_i}{\overline{FC}}\right)^2\right), \\ ET_{lower,i,(t,t+1)} &= ET_{soil,i,(t,t+1)} - ET_{upper,i,(t,t+1)}, \end{aligned} \quad (4)$$

where $ET_{soil,i,(t,t+1)}$ and $ET_{lower,i,(t,t+1)}$ are evapotranspiration in grid cell *i* during the daily time step $(t,t+1)$ from the whole soil profile and the lower layer, respectively, in millimetres; $S_{abs,RT,i,t}$ is the absolute retention parameter for the root zone of soil in day *t* in grid cell *i* in millimetres, which is calculated as $S_{abs,RT,i,t} = S_{abs\_mx,i}\cdot D_{RT,i,t} / Z_i$, where Z_i is the soil depth to restrictive layer in millimetres; $D_{RT,i,t}$ is the depth of root zone in day *t* in grid cell *i* in millimetres. The root zone depth of forests is set to be equal to the soil depth, the root zone depth of grassland and pastures is set to the smaller value between 300 mm and the soil depth, and the root zone depth of agricultural field is defined by users.

The moisture content in the saturated layer (M_{bal}) is controlled by the variation of water table depth and is calculated assuming homogeneous soil properties across layers:

$$M_{\mathrm{bal},i} = S_{\mathrm{abs\_mx},i} \cdot \left(1 - \frac{D_i}{Z_i}\right), \tag{5}$$

where $S_{\mathrm{abs\_mx},i}$ is the maximum value of absolute retention parameter in grid cell i, and D_i is the depth to water table in grid cell i in millimetres and is represented as a function of the STI according to the concept of TOPMODEL (Beven, 1995):

$$D_i = \overline{D} - \frac{1000}{f_{\mathrm{soil}}}\left(\mathrm{STI}_i - \overline{\mathrm{STI}_{\mathrm{ref}}}\right), \tag{6}$$

where $\overline{D}$ is the average water table depth of the reference area, in millimetres; $\overline{\mathrm{STI}_{\mathrm{ref}}}$ is the average STI of the reference area; f_{soil} is a coefficient in the exponential decline of hydraulic conductivity with depth in m^{-1}. In TOPMODEL, the reference area means the whole watershed, and in DHM-WM, the reference area refers to the area of water bodies. To account for the spatial variation of $\overline{\mathrm{STI}_{\mathrm{ref}}}$, the whole watershed is delineated into small reference zones and the $\overline{\mathrm{STI}_{\mathrm{ref}}}$ is calculated as the average STI value of the water bodies (lakes/ponds/reservoirs/streams) within each zone. The water table distribution across the watershed landscape calculated by Equation 6 is illustrated as line a in Figure 2a.

With the water table variation, there is water exchange between landscape soil profiles and water bodies. According to the global water balance, the water content change in the soil profile (two layers as a whole) all over the watershed and the water content change in water bodies (represented as $\overline{D_t} - \overline{D_{t+1}}$) should be balanced as below:

$$\sum_i \left[\left(M_{i,t+1} + M_{\mathrm{bal},i,t+1}\right) - \left(M'_{i,t} + M_{\mathrm{bal},i,t} - \mathrm{ET}_{\mathrm{lower},i,(t,t+1)}\right)\right]/R_{\mathrm{water}} + \left(\overline{D_t} - \overline{D_{t+1}}\right) < Error, \tag{7}$$

where R_{water} is the number of grid cells of the water bodies. If $\left(\overline{D_t} - \overline{D_{t+1}}\right)$ is positive, that means there is return flow to lakes/ponds, which usually occurs in the wetting period; a negative $\left(\overline{D_t} - \overline{D_{t+1}}\right)$ means seepage from lakes/ponds to landscape soils, which usually occurs in the drying period. For each simulation day, with Equations 1–6, $\overline{D}$ is solved by iteration until the water balance shown in Equation 7 is satisfied with specific *Error*, set to be ±10 mm in DHM-WM.

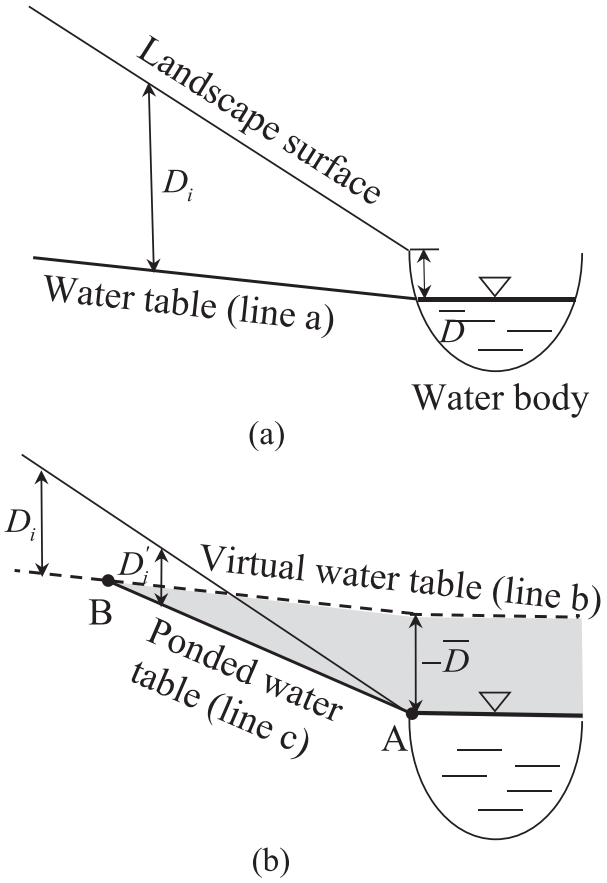

FIGURE 2 Illustration of water table distribution across landscape (a) in unsaturated moisture condition and (b) in saturated condition when saturation-excess runoff or subsurface stormflow occur. Notes: D_i is the water table depth on landscape grid cell i, and $\overline{D}$ is the average water table depth of the reference water bodies, both used in Equation 6; D_i' is the ponded water table depth on landscape grid cell i on saturated conditions

2.3 | Run-off generation

2.3.1 | Infiltration excess run-off

DHM-WM uses the Mishra-Singh CN method to calculate infiltration excess run-off depth as below:

$$Q_{i,(t,t+1)} = \frac{\left(P_{i,(t,t+1)} - Ia_{i,(t,t+1)} - Fc_{i,(t,t+1)}\right)\left(P_{i,(t,t+1)} - Ia_{i,(t,t+1)} - Fc_{i,(t,t+1)} + M_{i,t}\right)}{P_{i,(t,t+1)} - Ia_{i,(t,t+1)} - Fc_{i,(t,t+1)} + M_{i,t} + S_{i,t}}, \tag{8}$$

where $Q_{i,(t,t+1)}$ is the infiltration excess run-off depth generated on grid cell i during the daily time step $(t,t+1)$ in millimetres; $P_{i,(t,t+1)}$ is the precipitation, $Fc_{i,(t,t+1)}$ is the constant gravitational infiltration, and $Ia_{i,(t,t+1)}$ is the initial abstraction in grid cell i in the same time step, all in millimetres; $M_{i,t}$ is the antecedent soil moisture content on grid cell i of day t in millimetres. The initial abstraction $Ia_{i,(t,t+1)}$ is calculated as $\lambda \cdot S_{i,t}$, where λ is the initial abstraction coefficient and $S_{i,t}$ is the retention parameter in grid cell i of day t in millimetres. Since only the upper unsaturated layer is active in surface processes, the $M_{i,t}$ and $S_{i,t}$ in Equation 8 denote the moisture content and the retention parameter for the unsaturated layer.

The Fc is estimated as $Fc = f_c \cdot t_e$, where f_c is the gravitational infiltration rate in mm/hr and t_e is the time duration of effective precipitation in hours (Mishra & Singh, 2003). In DHM-WM, f_c is assumed to be linearly related to saturated hydraulic conductivity (K_S) as $f_c = f_{c0} \cdot K_S$, where f_{c0} is the gravitational infiltration parameter that requires calibration.

2.3.2 | Saturation excess run-off or subsurface flow

If the water body surface exceeds the threshold, saturation excess run-off or subsurface flow is simulated. Currently, the threshold is set to be the land surface elevation adjacent to water bodies. In this case, the $\overline{D}$ is forced to be 0 mm if its solved value from global water balance Equation 7 is less than 0 mm. Meanwhile, the extra water due to the forced $\overline{D}$ (shaded area in Figure 2b) becomes saturation excess run-off on rainy days or subsurface stormflow on no-rain days. In Figure 2b, line b (the dashed line) is the virtual water table distribution associated with a negative $\overline{D}$ solved by water balance

in Equation 7. In reality, when the water body surface reaches the adjacent land surface, subsurface lateral movement is restricted. This causes the water to start ponding from around the water body (point A) and then further away, until the ponded water table (line c) intersects with the virtual water table (line b) at point B. The actual water table distribution is line c between points A and B, and line b further away from point B. The ponded water table depth $D_i^{'}$ (line c) is also calculated with Equation 6 but with an adjusted $f^{'}_{soil} = f_{soil} \cdot (1 + k_f)$, where k_f is the adjustment parameter for f_{soil} on ponding condition that needs calibration.

2.4 | Routing

2.4.1 | Routing for surface flow

For surface run-off routing, DHM-WM calculates the travel time on a grid cell basis. For grid cells with overland flow, the steady state kinematic wave approximation is combined with Manning's equation (Chow, Maidment, & Mays, 1988) to estimate travel time $To_{i,(t,t+1)}$ for grid cell i at time step $(t,t+1)$ as follows:

$$To_{i,(t,t+1)} = q_{i,(t,t+1)}{}^{-0.4} \left(\frac{L_i{}^{0.6} n_i{}^{0.6}}{\tan(\beta_i)^{0.3}} \right), \quad (9)$$

where L_i and $\tan(\beta_i)$ are length and slope of the grid cell i, in metres and m/m, respectively; n_i is the Manning's roughness coefficient of the grid cell i; and $q_{i(t,t+1)}$ is the surface flow from grid cell i during the time step in m/s. For grid cells representing streams and channels, the travel time $Tc_{i,(t,t+1)}$ for grid cell i at time step $(t,t+1)$ is calculated by combining Manning's equation and the continuity equation as (Melesse & Graham, 2004; Muzik, 1996):

$$Tc_{i(t,t+1)} = \frac{L_i \cdot n_i{}^{0.6} \cdot W_i{}^{0.4}}{\tan(\beta_i)^{0.3} \cdot q_{acc\_i,(t,t+1)}{}^{0.4}}, \quad (10)$$

where W_i is the width of streams or channels in grid cell i, in metres; L_i, $\tan(\beta_i)$, and n_i are the same as in Equation 9; $q_{acc\_i,(t,t+1)}$ denotes the concentrated storm discharge during time step $(t,t+1)$ through grid cell i in m^3/s. In DHM-WM, flow direction is derived from a digital elevation model (DEM) using the D8 algorithm and used to track flow paths of surface run-off. Cumulative travel time of surface run-off is calculated by summing up the travel time through all grid cells along the flow path. The surface flow at the target outlet is then calculated as the sum of surface flow that can reach the outlet within the specific cumulative travel time.

2.4.2 | Routing for base flow

DHM-WM uses the same module in the Mishra-Singh CN method to calculate daily base flow (O_b) with gravitational infiltration (Fc) as water source and a single linear reservoir routing:

$$O_{b(t+1)} = 2 \cdot g_0 \cdot Fc_{(t,t+1)} + g_1 \cdot O_{b(t)} \quad (11)$$

where g_0 and g_1 are coefficients calculated as $g_0 = (1/K_b)/(2 + 1/K_b)$ and $g_1 = (2 - 1/K_b)/(2 + 1/K_b)$, respectively, in which K_b is the storage coefficient of base flow in d.

2.5 | Irrigation module as an option

Since irrigation impacts the spatial distribution of soil moisture by water transfer from water bodies to agricultural fields, a simple module accounting for irrigation is offered as an option of DHM-WM. A relative soil moisture level to stimulate irrigation practice (SM_{irrg}) is set by users. When the average upper layer soil moisture of all agricultural fields (SM_{ave}) is less than the defined threshold SM_{irrg} during the growing season, irrigation is applied by extracting water from ponds and reservoirs to agricultural fields that have a water deficit, raising the soil moisture to field capacity. The change in water content because of irrigation is also included in the global water balance Equation 7. If irrigation is not applied in the study watershed, the irrigation module can be turned off by setting SM_{irrg} to zero.

2.6 | Model development and operation

The DHM-WM is developed using Python scripts, and it is open for further modifications. The spatial data (both input and output data) are in ArcGIS raster format, and others are in text files. The output includes time series of soil moisture in the unsaturated layer, water table depth, and flows (surface flow, subsurface stormflow, base flow, and total streamflow) at user-selected sites, as well as spatial grids of daily run-off depth and travel time along flow paths. The computational time of DHM-WM depends on the watershed size, the grid cell size, the number of target sites selected to report, and the computer properties. For a watershed of 50 km^2 with a resolution of 30 m, three sites for which to report hydrographs, and five sites for soil moisture as in the case study below, DHM-WM simulation runs take about 1 hr per simulation year on a desktop with an Intel(R) Core(TM) i5 3.30 GHz CPU and 8.00 GB RAM. Modifications of the scripts such as using parallel algorithms would improve the computational efficiency.

3 | CASE STUDY

3.1 | Watershed description

The DHM-WM was applied to the 50-km^2 subwatershed I of the Little River watershed, which is located near Tifton, Georgia and is a benchmark research watershed monitored by United States Department of Agriculture–Agricultural Research Service–Southeast Watershed Research Lab (USDA-ARS-SEWRL; Bosch et al., 2007). The area is typical of the U.S. coastal region, with heavily vegetated streams, wetlands, and reservoirs. The major soil series are loamy sands with relatively high infiltration rates (Lowrance, Todd, & Asmussen, 1983; Rawls, Yates, & Asmussen, 1976). However, a shallow and relatively impermeable Hawthorn formation usually occurs in the soil profile (Cho, Bosch, Vellidis, Lowrance, & Strickland, 2012) and restricts the downward movement of water. Streamflow is strongly influenced by the shallow unconfined aquifer formed above this restrictive layer (Lowrance et al., 1983; Sheridan, 1997). Irrigation is applied occasionally, so the irrigation module of DHM-WM was used.

3.2 | Data preparation

Model input data include climate data (precipitation, temperature, and PET) on a daily scale, land cover map, soil map and soil properties, DEM, and hydrography. Data for model evaluation include daily time series of soil moisture and streamflow discharge. All data were provided by the USDA-ARS-SEWRL (Bosch, Sheridan & Marshall, 2007; Bosch & Sheridan, 2007). Among the data above, precipitation, land cover, soil, and DEM are gridded, on a resolution of 30 m. Gridded precipitation were interpolated with site data from 21 rain gauges (13 inside the study area and 8 nearby) by inverse distance weighting. Climate data covered the period of 2003–2009. For model evaluation, observed soil moisture at 300 mm depth from 5 gauges (MG31, MG34, MG37, MG39, and MG43) and observed streamflow from 3 gauges (watershed outlet I, as well as sites J and K that drain 2 nested tributaries) were collected from 2005 to 2009 (Figure 3a). For STI calculation, the watershed was divided into 109 reference zones (Figure 3 b), based on a principle that each significant lake, pond, and stream reach drains a separate reference zone. The $\overline{\mathrm{STI}_{\mathrm{ref}}}$ in Equation 6 is the average STI of the water body areas within each reference zone.

Soil properties were obtained from the SSURGO database and used to generate soil-related parameters needed by the model including hydrologic soil groups, soil depth to impervious layer (Z_{soil}), average saturated hydraulic conductivity (K_{soil}), average total porosity (P_t), and average effective porosity (P_e). Parameter Z_{soil} is determined by checking the saturated hydraulic conductivity with depth, and an impervious layer is defined as one with conductivity below 10 mm/hr. P_t and P_e are calculated based on soil texture data (http://web.ead.anl.gov/resrad/datacoll/porosity.htm). The values of soil parameters are listed in Table 1. The PET data were estimated using the other climate data monitored from sites with grass land cover. Crop coefficients (K_c) were used to convert the grassland-referenced PET to PETs of different land covers. Based on the FAO 56 document (Allan, Pereira, Raes, & Smith, 1998), the K_c of forests was set to 1.10 and 0.80 for the growing season and inactive season, respectively, since most of the forests are deciduous; the K_c of agricultural fields (mainly cotton and peanuts) was set to be 1.15 and 0.70 for the growing and fallow season, respectively; and the K_c of water bodies was set to 1.05.

3.3 | Sensitivity analysis

Sensitivity analysis was conducted from 2005 to 2006 to explore model parameter impacts on simulated results. All model parameters are as summarized in Table 2, and all except storage coefficient for base flow (K_b) and soil moisture level for irrigation (SM_{irrg}) were analysed. Each parameter was evaluated separately using the one-at-a-time scheme; thus, only the parameter being analysed at any one time was changed while other parameters remained at baseline values during simulation.

3.4 | Model calibration and evaluation

To make the variables (M, M_{bal}, and $\overline{D}$) representative to the moisture and water level condition of the specific time and space of the study watershed, a warm-up period covering both dry and wet seasons is needed for DHM-WM. For the case study, a 2-year period (2003–2004) was used for warm-up, and the calibration period and validation period were 2005–2006 and 2007–2009, respectively. Model performance was evaluated by checking water balance and the reasonableness of base flow percentage as well as comparing the observed and simulated data of soil moisture at the five gauges and streamflow at

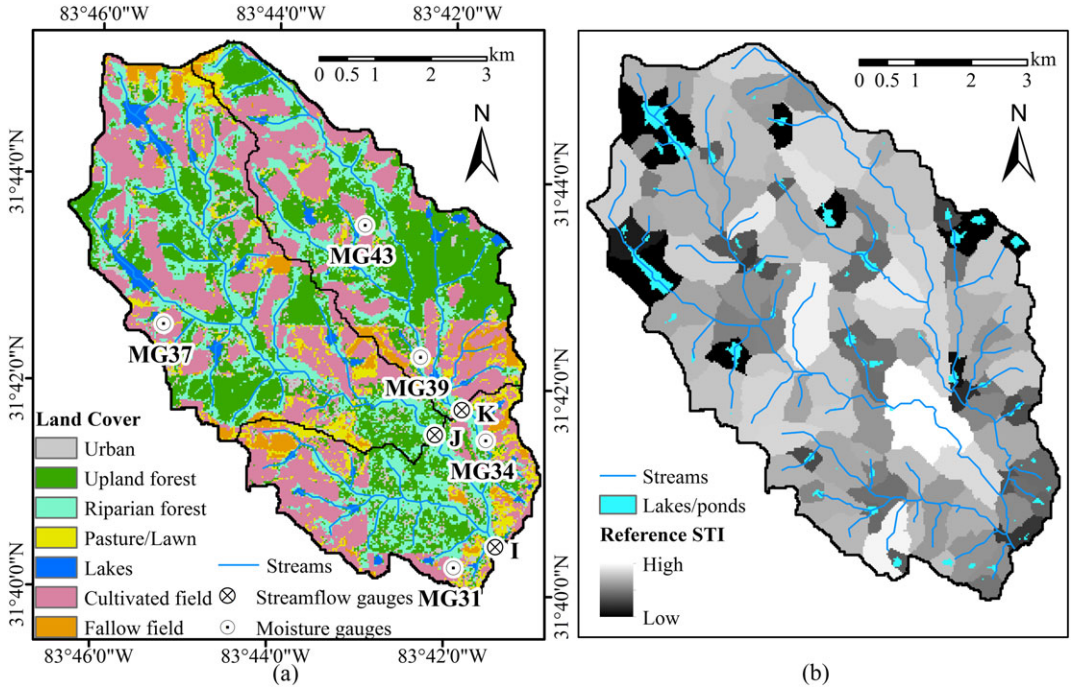

FIGURE 3 (a) Land cover map and the monitoring gauges of the study watershed and (b) the distribution of reference soil topographic index ($\overline{\mathrm{STI}_{\mathrm{ref}}}$ in Equation 6) within each reference zone

TABLE 1 Soil-related parameters used in distributed hydrologic model for watershed management in Little River Experimental Watershed

Soil name	HSG	Z_{soil} (m)	K_{soil} (m/day)	P_e	P_t
Tifton C	B	1.31	2.53	0.26	0.40
Dothan	C	1.44	0.93	0.25	0.40
Lakeland	A	2.04	4.38	0.30	0.39
Water	D	0.03	14.63	0.28	0.40
Tifton A	B	1.59	1.87	0.25	0.40
Tifton B	B	1.54	1.86	0.26	0.40
Fuquay	B	0.79	3.26	0.29	0.40
Leefield	B	1.30	3.94	0.28	0.40
Stilson	B	1.65	3.71	0.27	0.40
Sunsweet	C	0.36	0.30	0.19	0.41
Cowarts C	C	0.94	0.60	0.24	0.40
Cowarts C2	C	0.79	0.53	0.22	0.41
Alapaha	D	1.48	3.44	0.28	0.40
Esto B	C	0.31	0.38	0.24	0.41
Cowarts B2	C	0.79	0.53	0.22	0.41
Cowarts B	C	0.94	0.60	0.27	0.40
Kinston & Osier	D	1.61	3.81	0.26	0.41
Esto C	C	0.31	0.38	0.24	0.41
Ardilla	C	1.25	1.42	0.24	0.40

the three gauges. To check the reasonableness of base flow percentage, the simulated value was compared to the observed value calculated from observed streamflow data using the Web-based Hydrograph Analysis Tool (WHAT; Lim et al., 2005), an online base flow separation tool providing three commonly used filters. The recursive digital filter (Eckhardt, 2008) was used with the BFI_{max} parameter set to 0.80 and the recession parameter set to 0.98. For streamflow, a visual comparison of time series was performed and performance statistics including the coefficient of determination (R^2) and the Nash-Sutcliffe coefficient (E_{NS}) on both daily and monthly scales, and the overall percent bias (P_{bias}) were computed. E_{NS} greater than 0.65 and P_{bias} less than 15% were regarded as good performance; E_{NS} greater than 0.50 and P_{bias} less than 25% were regarded as satisfactory (Moriasi, Gitau, Pai, & Daggupati, 2015; Moriasi et al., 2007). For soil moisture comparison, R^2 on a daily scale and P_{bias} were calculated to assist visual assessment of time series graphs.

4 | RESULTS

4.1 | Verification of model parameters

4.1.1 | Maximum absolute retention parameter: S_{abs_mx}

The maximum value of the absolute retention parameter S_{abs_mx} should represent the maximum water capacity or the porosity that can be filled up by water. So, the baseline value of watershed average S_{abs_mx} was set to be 552 mm, a value equal to the average maximum watershed storage (552 mm) which is the product of average soil depth (1.38 m) and the average soil porosity (0.40). The calibrated S_{abs_mx} was greater than the baseline value, indicating the watershed is more likely to store water rather than generate run-off. This is reasonable since the watershed generally had a high soil infiltration rate.

The S_{abs_mx} is a very sensitive parameter as illustrated in Figure 4. As S_{abs_mx} increased, there was a decreasing trend of streamflow and increasing trend of ET. Figure 4d also indicated a significant impact of S_{abs_mx} on daily streamflow variation. It should be noted that Figure 4d was mainly used to indicate daily scale simulation response to parameter changes; the relationship between daily R^2 of streamflow and parameters may change with a different baseline.

4.1.2 | Parameters controlling subsurface water table variation and saturation excess run-off: f_{soil} and k_f

The subsurface water table variation across the watershed is controlled by STI and the exponential decline coefficient of hydraulic conductivity (f_{soil}). A larger f_{soil} resulted in less streamflow, greater ET, and a greater base flow percentage (Figure 4). A larger f_{soil} means less variance of subsurface water table. In this condition, water tends to distribute across the watershed rather than concentrate on lowland areas around water bodies, which increases ET in general and reduces the possibility of saturation excess run-off.

Parameter k_f, the adjustment parameter for f_{soil}, had little impact on the annual average simulation results. Yet, parameter k_f changed daily streamflow variation, which was indicated in daily R^2 variation (Figure 4d). In addition, parameter k_f impacts the spatial distribution of surface run-off. Figure 5 showed the surface run-off distribution generated on March 31, 2005 (a wet day when saturated-excess run-off was simulated) with different k_f while other parameters were the

TABLE 2 Summary of all parameters that need calibration in distributed hydrologic model for watershed management

	Description	Range	Baseline value	Calibrated value
S_{abs_mx}	Maximum value of absolute retention parameter (mm)	>0	Watershed average: 552	Watershed average: 627
λ_{MAX}	Maximum value of initial abstraction coefficient	0–0.30	Growing season: 0.16 Fallow season: 0.12	Growing season: 0.21 Fallow season: 0.16
f_{c0}	Gravitational infiltration rate coefficient	0–1.000	0.012	0.018
K_b	Storage coefficient of base flow (d)	>0.5	7	7
f_{soil}	Exponential decline coefficient of conductivity with soil depth (m^{-1})	1.0–20.0	9.0	6.2
k_f	Adjustment parameter for f_{soil} on saturated condition	0–1.00	0.30	0.14
$\overline{tM}$	Watershed average time to drain for moisture loss estimation (h)	0–200	50	24
SM_{irrg}	Relative soil moisture level below which irrigation is applied	0–1.000	0.213	0.251

Note. Parameter S_{abs_mx} is distributed, various for different soil–land cover combinations; other parameters are lumped, the same across the watershed.

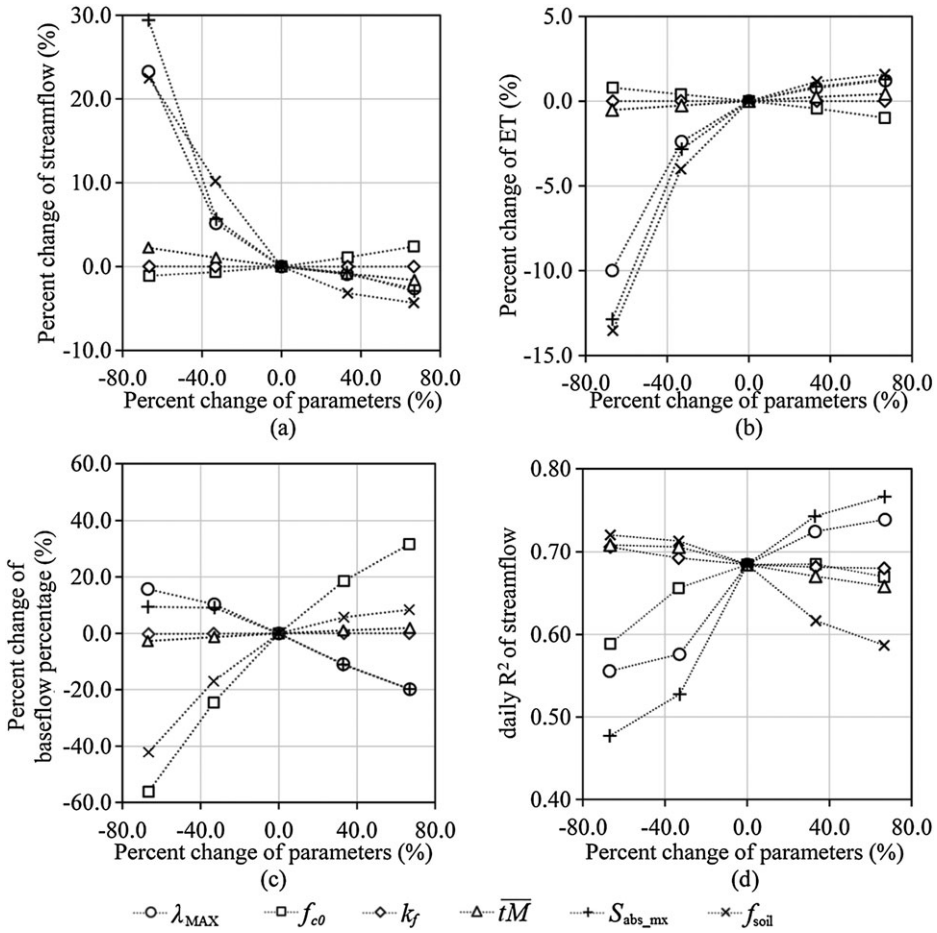

FIGURE 4 Parameter impacts on simulated (a) annual streamflow, (b) annual evapotranspiration (ET), (c) average base flow percentage, and (d) daily R^2 of streamflow at the watershed outlet. Note: Parameter descriptions can be found in Table 2

same. As k_f decreased, the area generating higher surface run-off expanded. The most apparent difference was highlighted in Figure 5. As expected, average surface run-off depths increased with decreased k_f (6.0, 6.2, and 6.8 mm for k_f values of 0.5, 0.3, and 0.1, respectively).

4.1.3 | Soil moisture loss parameter: $\overline{tM}$

One parameter ($\overline{tM}$) is used in DHM-WM to control the soil moisture loss velocity from the upper layer to the lower layer. As $\overline{tM}$ becomes larger, the extra water stays in the upper layer longer. This impact only occurs on specific days when soil moisture is above field capacity. Hence, it had only a slight impact on the annual outputs of streamflow yield, ET, and base flow percentage (Figure 4a-c). It, however, changed the hydrologic response during specific days as indicated by the daily variation of streamflow shown in Figure 4d.

4.1.4 | Other parameters

The maximum value of the initial abstraction coefficient, λ_{MAX} adjusts initial abstraction directly. Since initial abstraction becomes ET or infiltrates into soils, ET and soil moisture content increased with larger λ_{MAX} value. In addition, larger λ_{MAX} reduced streamflow and decreased base flow percentage. The gravitational infiltration rate parameter f_{c0} was influential to the base flow percentage as expected but did not show big impacts on streamflow and ET.

4.2 | Soil moisture

The model performance in simulating soil moisture variation was checked by comparing the observed relative moisture content and the simulated values ($M_{i,t}/S_{abs,i,t}$) at the five moisture gauges, all located on grassland (Figure 6). It should be noted that there was a difference in expected values due to measurement at a point (300-mm depth) versus simulation of full vertical profile of the unsaturated layer, as indicated by the P_{bias}. With this difference, the daily R^2 showed that the patterns and trends of simulated soil moisture matched well with the observed data for all sites except MG43. The closeness of match also varied with the depth of the unsaturated layer (indicated by the shaded colour in Figure 6). Specifically, during the drying periods when the water table dropped, the simulated moisture generally decreased more slowly than the observed moisture for all sites. There may be two reasons for this. One is the observed moisture at 300-mm depth is within the root zone and dries up due to plant uptake more quickly, while the simulated moisture includes parts of zones without roots. The other reason is the downward percolation; when water moves downward, the 300-mm depth soil dries up while the moisture content in the upper layer does not change since the percolated water is still within the unsaturated layer. In general, model performance in simulating soil moisture magnitude and variation was good for MG31 and MG34, fair for MG37 and MG39, and not satisfactory for MG43. This

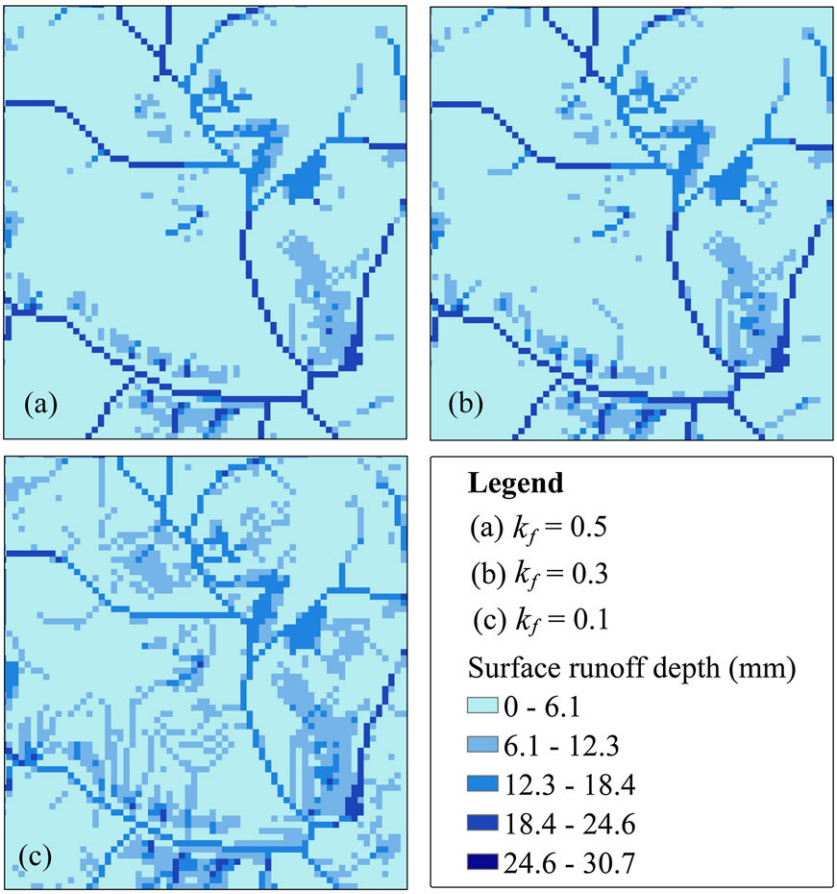

FIGURE 5 The impact of the adjustment parameter for f_{soil} in saturated condition (*kf*) on the spatial distribution of surface run-off (enlarged view of a part of the watershed)

is acceptable since previous research pointed out MG31 and MG34 were representative of the soil moisture conditions of the watershed, and MG43 was a bit of an outlier (Bosch, Lakshmi, Jackson, Choi, & Jacobs, 2006).

In addition, the impact of soils on moisture variation was simulated by DHM-WM. Figure 6 showed that the moisture of Fuquay soil (MG34 and MG39) generally peaked and dropped more quickly than the Tifton soil (MG31, MG34, and MG43). This was reasonable since the unsaturated layer of Fuquay soil contains less clay and has a smaller field capacity. That makes the soil easier to drain and more likely to evaporate and transpire, which results in quicker moisture loss. On rainy days, with less antecedent moisture after drainage and ET, the Fuquay soil infiltrates more water and has quicker moisture gains. The shaded area in Figure 6 implied that there was always a saturated layer that occurred in the 1.54-m depth soil profile of Tifton soil (varying from 0.5- to 1.3-m depth), while a saturated layer only occurred on specific wet days in Fuquay soil with a shallower soil depth (0.79 m).

4.3 | Water balance and base flow percentage

Water balance and the reasonableness of base flow percentage were checked. The annual watershed storage (difference between precipitation and water yield to ET and streamflow) varied from −72 to 57 mm (Table 3) during the simulation period. Generally, watershed storage aligned with the simulated variation of water table and moisture content in soils. The year with the greatest water release from the watershed (2006) also saw the largest decrease of water table and soil moisture content. The largest watershed storage occurred in the year 2009 when there was the greatest increase of soil moisture, but water gains simulated in water bodies (indicated in the increase of water table) were less than for year 2008. The deviation of the positive relationship between watershed storage and water table variation during 2007–2009 may be caused by the accumulation of simulated daily errors of water table depth through the global water balance Equation 7. During the 2005–2009 simulation period, the net watershed storage was 11 mm, but no water gains were simulated in water bodies and landscape soils. This overall error was acceptable, indicating that the water balance was reasonably represented by DHM-WM.

The base flow ratio simulated by DHM-WM averaged 0.53 for the simulation period (2005–2009) with a range from 0.45 to 0.75 for each year. The results by base flow separation using observed data had the same average value of 0.53 but a narrower range of 0.47–0.66. The higher simulated base flow percentage occurred on relatively drier years as expected, since dry days tended to have less surface run-off and a higher base flow percentage. However, the simulated base flow percentages of 2007 and 2008 exceeded the observed range, probably caused by simulated flow during some very dry days when no observed flow occurred. This phenomenon will be further discussed in the time series results of streamflow below.

4.4 | Streamflow

Statistics showed that DHM-WM generally performed well in simulating streamflow at all three monitoring sites (Table 4). For subwatershed J and the final outlet I, model performance for streamflow was very good for both calibration and validation periods. For subwatershed K,

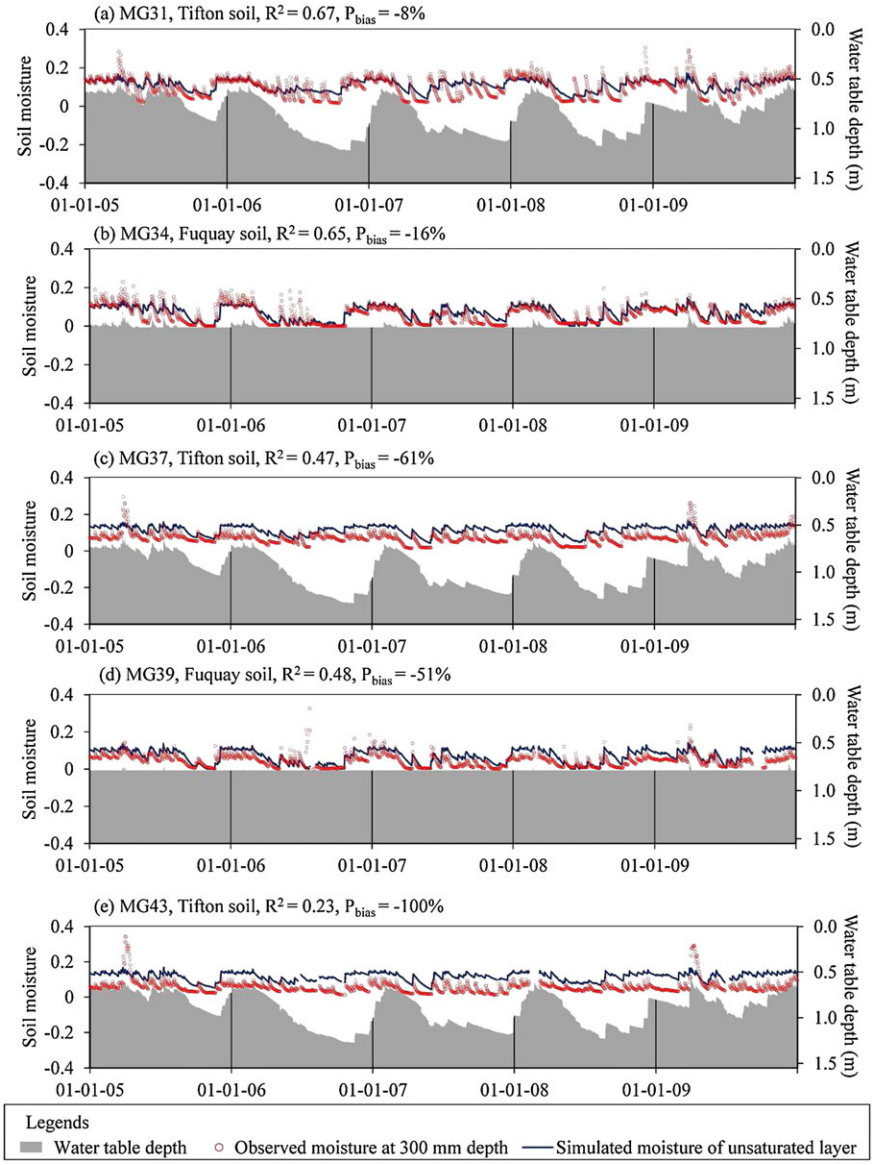

FIGURE 6 Comparison of observed and simulated relative soil moisture at the five monitoring gauges, along with simulated water table depth

the daily E_{NS} was satisfactory, but its general performance was still good with a monthly E_{NS} of 0.67 and a P_{bias} of −12% for the calibration period and even better for the validation period. Table 4 shows P_{bias} for different moisture conditions with different run-off types. Compared to the P_{bias} for all periods, the P_{bias} for the saturated periods did not show an apparent difference. However, the model seemed to overestimate streamflow during the wetting periods and underestimate during the drying periods; and only infiltration excess run-off was simulated in both periods. This phenomenon was further analysed by comparing graphs of time series.

Generally, the peaks and recessions of streamflow were well simulated (Figure 7). However, discrepancies were observed in several rainfall storms (larger than 50 mm per day) during the early wetting periods that did not produce streamflow in the watershed, but simulated results had streamflow response. Also, during the latter part of stormflow seasons, there was underestimation for several storms. These graphic discrepancies align with those shown in P_{bias} above. Actually, this observation was also mentioned in a study on development of Gridded SWAT in the same watershed (Rathjens et al., 2015). These authors argued that this was because the CN method used by SWAT could not represent saturation excess run-off. In this study, DHM-WM simulated both infiltration and saturation excess run-off. Still, it might overestimate infiltration excess run-off during the wetting period and miss saturation excess run-off during the drying periods due to the simulated water table dropping too quickly. One reason might be the widespread lakes and ponds in the watershed, which temporarily stored the surface run-off that flowed into them during the wetting period and extended the saturated periods longer than what was simulated. Based on a flow accumulation analysis with a flow direction map in which the lakes/ponds are omitted, run-off from 39.2% of the watershed flows into lakes/ponds before reaching watershed outlet I. Nevertheless, the streamflow response simulated by DHM-WM when the storms did not lead to observed streamflow was much less than that with similar storms during the later wet periods when saturation excess run-off occurred (Figure 7). Another probable reason was that the calibrated parameters set to prioritize daily, monthly and overall statistics were not ideal for consistent representation of wetting and drying periods. In fact, the underestimation for the drying period could be a compensation for the overestimation for the wetting period to obtain best overall statistics.

TABLE 3 Statistics of annual precipitation and simulated results in the case study area

	Precipitation (mm)	ET (mm)	Streamflow (mm)	Watershed storage (mm)	Variation of water table (mm)	Variation of average soil moisture	Base flow ratio
2005	1218	779	451	−12	−40	−0.03	0.46
2006	885	772	186	−73	−282	−0.13	0.58
2007	933	801	110	22	+43	+0.04	0.75
2008	1048	788	244	17	+162	+0.04	0.70
2009	1425	823	546	57	+117	+0.08	0.45
2005–2009	5509	3962	1536	11	0	0.00	0.53

Note. ET = evapotranspiration.

TABLE 4 Distributed hydrologic model for watershed management performance in simulating streamflow

Monitoring sites	Daily		Monthly		P_{bias} (%)	P_{bias} for SAT (%)	P_{bias} for INF_WET (%)	P_{bias} for INF_DRY (%)
	R^2	E_{NS}	R^2	E_{NS}				
Calibration (2005–2006)								
K	.71	.56	.69	.67	−12	−17	−26	10
J	.75	.75	.94	.89	13	13	3	20
I	.78	.78	.94	.91	9	7	−2	25
Validation (2007–2009)								
K	.86	.85	.90	.87	−8	−13	−17	13
J	.83	.83	.83	.83	−9	−8	−16	0
I	.80	.79	.80	.80	9	0	9	31

Note. SAT refers to the saturated periods when saturation excess run-off and subsurface stormflow occurred. E_{NS} = Nash-Sutcliffe coefficient; P_{bias} = percent bias

INF_WET refers to the wetting periods when only infiltration excess run-off was simulated;

INF_DRY refers to the drying periods when only infiltration excess run-off was simulated.

4.5 | Spatial details

Figure 8 shows the spatial details of simulated soil moisture and surface run-off on a typical wet day and a typical dry day with similar precipitation. Figure 8a,b is for April 2, 2009 when there was a 67-mm precipitation event, and the water elevation in water bodies reached the surface. Figure 8c,d is for the dry day, November 15, 2006 when there was a 62-mm precipitation and the simulated water table in water bodies was 594 mm below the surface. The average relative soil moisture contents of the watershed were 0.75 and 0.44 for the wet and dry days, respectively. On the wet day, about 33% of the watershed had a relative soil moisture greater than 0.8, while the area for the dry day was only 2% and included only open water bodies. Despite the great difference of soil moisture content, the general spatial distribution of soil moisture for the 2 days was quite similar (Figure 8a,c). The soil moisture distribution was largely controlled by the relative position within the landscape (Figure 3b). The reference zones with lakes and ponds had lower $\overline{STI_{ref}}$ and higher soil moisture content. This is reasonable since these reference zones have a larger area of water bodies with shallower water tables. Within each reference zone, the lower areas nearer to streams and lakes/ponds were wetter than the upland areas further away, as suggested by variable source area hydrology theory.

As expected, the wet day generated much more surface run-off than the dry day (Figure 8b,d). On the wet day, the average surface run-off was 34.5 mm and on the dry day it was 3.3 mm. Comparing the distribution of simulated surface run-off and soil moisture, areas with higher soil moisture content generally had higher potential to generate surface run-off. This relation was quite apparent for the wet day. The areas around lakes/ponds and streams generated the highest surface run-off, and surface run-off was reduced further away from these areas similar to the distribution of soil moisture content. This was because in this very wet condition, there was a large area that was previously very wet and easily saturated during the storm. Even in the upland areas that did not generate saturation excess run-off, infiltration excess run-off was larger since less water can infiltrate in wet soils (Equation 8).

By contrast, the relation between surface run-off and soil moisture was not that significant for the dry day. The relatively high surface run-off areas (shown in dark green and blue in Figure 8d) were mostly in the area with normal soil moisture condition (0.4–0.6). However, these areas coincided with the soils having relatively low hydraulic conductivity based on soil property data. The low infiltration and percolation rate made them likely to generate infiltration excess run-off even in relatively dry and normal conditions. Besides soils, surface run-off was also impacted by land cover represented by the S_{abs_mx} parameter of the model, as highlighted in the square in Figure 8d. The forests alongside the stream generated lower surface run-off than surrounding agricultural areas. Besides soil and land cover, surface run-off generation was also impacted by rainfall distribution. Although the areas illustrated in the circles in Figure 8d were in similar soil moisture condition, in the lower left circle even the agricultural lands generated little run-off because of the relatively low rainfall of about 57 mm. The areas

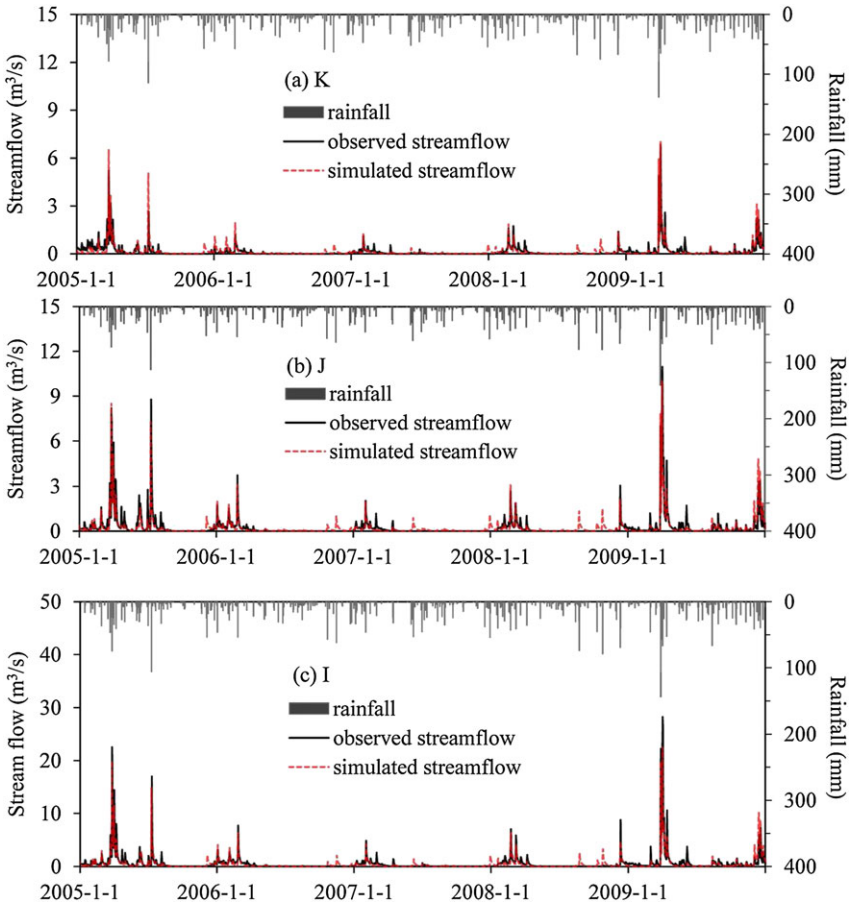

FIGURE 7 Comparison of observed and simulated daily streamflow at monitoring gauges (a) K, (b) J, and (c) I

in the upper right one generated much more run-off on both agricultural and forest lands due to a relatively high rainfall of about 75 mm. The impacts of local characteristics, rainfall, soil properties, and land cover also existed for the wet day but were outweighed by the soil moisture impact to a large extent.

5 | DISCUSSION

5.1 | The capability of representing different run-off generation mechanisms

The conceptualization of DHM-WM simulates both infiltration excess and saturation excess run-off through distributed soil moisture estimation accounting for both local and global water balance. The run-off for unsaturated days was simulated as infiltration excess run-off, and saturation excess run-off was also simulated when the simulated water table reached a threshold. This reduced the discrepancy of overestimating surface flow during the early wetting period and underestimating during the later wet season in the case study. This discrepancy would be further minimized or eliminated by representation of the temporal surface flow storage in lakes and ponds, or including more specific indicators for model calibration, such as separating P_{bias} for the wetting period and the drying period.

The case study also showed that the spatial distribution of surface run-off on dry days was mostly controlled by local factors (rainfall, soil, and land cover) and was largely determined by global watershed characteristics (relative position and hydrologic connectivity) on wet days when soil moisture impact outweighed other factors. This was reasonable since saturation excess run-off that occurred on wet days was more related to global watershed characteristics. In this sense, by representing both infiltration excess and saturation excess run-off mechanisms, DHM-WM reasonably simulated the spatial distribution of surface run-off.

For arid regions with poorly drained soils, subsurface water movement is less significant and only local water balance may be adequate to simulate soil moisture variation. For watersheds where all lands are pervious and well-drained, infiltration excess run-off is not likely to occur so that models with only saturation excess run-off mechanism may be adequate. With both local and global water balance accounted for, DHM-WM is most suitable for watersheds with both run-off mechanisms, where subsurface lateral movement of water makes part of the watershed likely to saturate, and meanwhile, there are impervious or poorly drained land surfaces prone to infiltration excess run-off.

5.2 | The potential for determining fine-scale CSAs and assisting cost-effective management

The reasonable spatial details of run-off generation simulated by DHM-WM provide sound basis for further identification of fine-scale pollutant CSAs since hydrology plays an overwhelming role on nutrient transfers (Kleinman et al., 2011). The travel times of run-off across flow paths are reported as intermediate outputs, which can

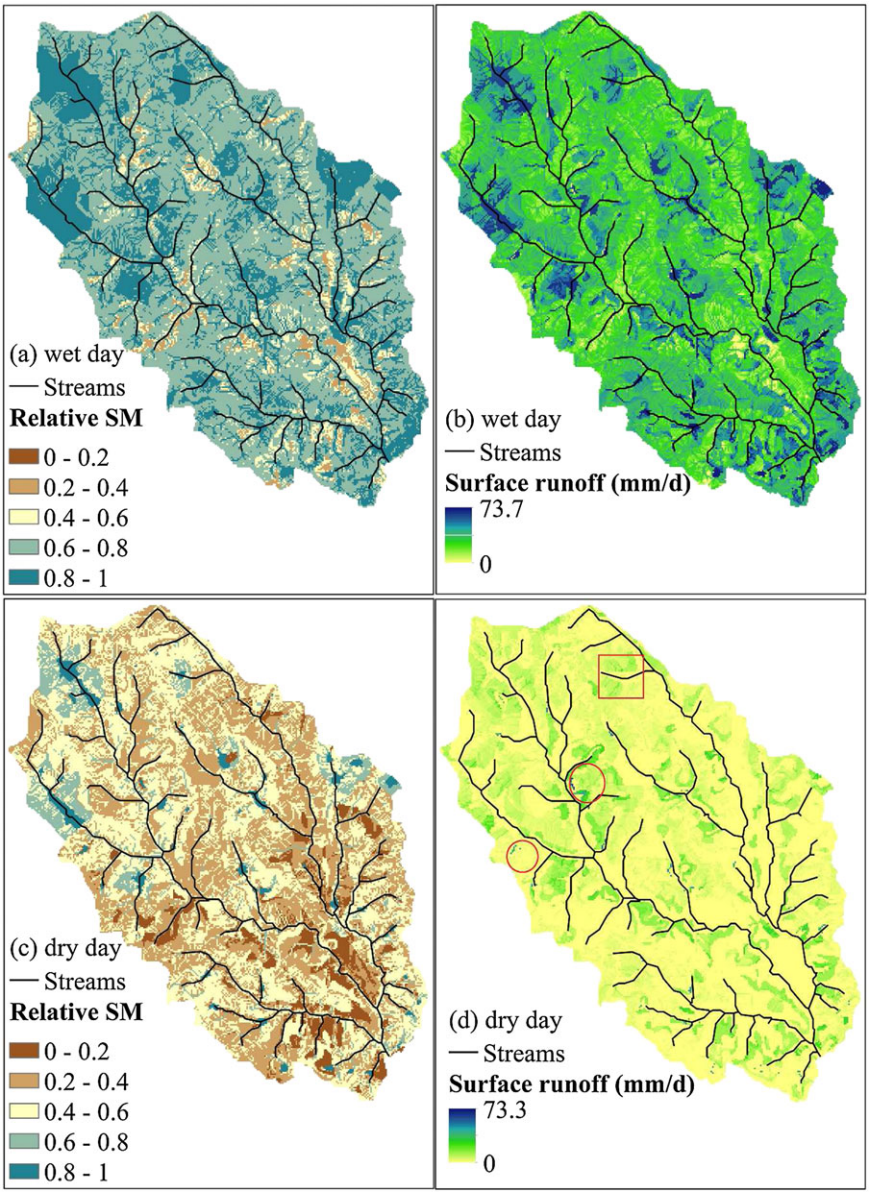

FIGURE 8 Spatial details of (a) relative soil moisture (SM) and (b) surface run-off for a wet day (2009-04-02), (c) relative SM, and (d) surface run-off for a dry day (2006-11-15) simulated by distributed hydrologic model for watershed management. Note: The square and the circles in figure (d) are highlighted areas that are discussed in the text

facilitate further estimation of water quality elements since sediment and nutrient transfers are greatly impacted by their travel routes and travel time (Chescheir, Gilliam, Skaggs, & Broadhead, 1991; Hoffmann, Kjaergaard, Uusi-Kämppä, Hansen, & Kronvang, 2009; Uusi-Kämppä, Braskerud, Jansson, Syversen, & Uusitalo, 2000). In addition, all the spatial information is provided on a grid cell basis, which is easy to connect to management units and to facilitate developing conservation measures.

5.3 | Model advantage and perspectives for further improvements

DHM-WM searches for simplification of hydrologic complexity by representing the critical factor (soil moisture variation) to run-off generation with empirical equations and limited parameters. There are at most eight parameters needing calibration (listed in Table 2), and if irrigation is not applied in the study watershed, there are only seven calibrated parameters. This reduces the difficulty in using the model. In addition, it reduces the uncertainty of getting good statistical results in streamflow at the watershed outlet even while internal state variables and hydrological processes are misrepresented, which is a common concern for distributed hydrologic models, especially those with a large number of parameters (Seibert & McDonnell, 2003). The case study also used multivariable and multisite evaluation (Bergström, Lindström, & Pettersson, 2002; Cao, Bowden, Davie, & Fenemor, 2006) to reduce the aforementioned uncertainty, which proved the reasonableness of the general concepts of DHM-WM and its ability in simulating spatial and temporal variations of soil moisture as well as streamflow.

Admittedly, the simplification of DHM-WM means some processes (snow, soil freezing, impacts of agricultural management practices, and reservoir management) are not accounted for; and some processes such as variability of soil hydrologic characteristics, seepage, and return flow are included in other processes. If any of these processes is critical to a specific watershed, further modifications would be developed.

6 | CONCLUSIONS

A simple grid-cell-based DHM-WM was developed focusing on soil moisture variation and run-off generation. The model was applied on the 50-km^2 watershed I of the Little River watershed in Georgia, USA. When tested with multisite and multivariable evaluation, DHM-WM proved to satisfy water balance and simulate hydrologic components, spatial and temporal variations of soil moisture, and streamflow reasonably well. Spatial details of modelling results indicated that infiltration excess run-off simulated by DHM-WM was generally controlled by local characteristics (precipitation, soil, and land cover) on unsaturated days. Global watershed characteristics (relative position and hydrologic connectivity) largely outweighed local characteristics when soil moisture reached a threshold and both infiltration and saturation excess run-off occurred. DHM-WM provides a new perspective on simulating complex distributed hydrology using simple empirical equations and limited parameters. As a simple grid-cell-based model representing both infiltration and saturation excess run-off, DHM-WM is a promising supplement to current models for determining fine-scale hydrologically based critical source areas and developing best management practices.

ACKNOWLEDGMENTS

This work was supported by the National Key Research and Development Program of China under Grant No. 2016YFD0800500, the National Natural Science Foundation of China under Grant No. 41471433, the Youth Innovation Promotion Association CAS under Grant No. 2016304, and the China Scholarship Council under Grant No. 201504910561. Datasets for the Little River Experimental Watershed were provided by USDA-ARS-SEWRL. Mention of company or trade names is for description only and does not imply endorsement by the USDA. The USDA is an equal opportunity provider and employer. We express our gratitude for the efforts of anonymous reviewers.

ORCID

Liang Zhang http://orcid.org/0000-0002-9074-1034

REFERENCES

Allan, R. G., Pereira, L. S., Raes, D., & Smith, M. (1998). Crop evapotranspiration-guidelines for computing crop water requirements-FAO irrigation and drainage paper 56. FAO, 56.

Arnold, J. G., Srinivasan, R., Muttiah, R. S., & Williams, J. R. (1998). Large area hydrologic modeling and assessment part I: Model development. *JAWRA Journal of the American Water Resources Association*, *34*, 73–89.

Becknell, B. R., Imhoff, J. C., Kittle, J. L., Donigian, A. S., & Johanson, R. C. (1993). Hydrological simulation program: FORTRAN, user's manual for release 10. US EPA.

Bergström, S., Lindström, G., & Pettersson, A. (2002). Multi-variable parameter estimation to increase confidence in hydrological modelling. *Hydrological Processes*, *16*, 413ess.

Beven, K. (1995). TOPMODEL. In V. P. Singh (Ed.), *Computer models of watershed hydrology* (pp. 627–668). Highlands Ranch, Colorado: Water Resources Publications.

Bieger, K., Arnold, J. G., Rathjens, H., White, M. J., Bosch, D. D., Allen, P. M., … Srinivasan, R. (2017). Introduction to SWAT+, a completely restructured version of the soil and water assessment tool. *Journal of the American Water Resources Association*, *53*, 115–130.

Bingner R., & Theurer F. (2001). AnnAGNPS technical processes: Documentation version 2. Agricultural Research Service, US Department of Agriculture, Oxford, MS.

Boll, J., Brooks, E. S., Crabtree, B., Dun, S., & Steenhuis, T. S. (2015). Variable source area hydrology modeling with the water erosion prediction project model. *Journal of the American Water Resources Association*, *51*, 330–342. https://doi.org/10.1111/1752-1688.12294

Bosch, D. D., Lakshmi, V., Jackson, T. J., Choi, M., & Jacobs, J. M. (2006). Large scale measurements of soil moisture for validation of remotely sensed data: Georgia soil moisture experiment of 2003. *Journal of Hydrology*, *323*, 120–137.

Bosch, D. D., Sheridan, J. M., & Marshall, L. K. (2007). Precipitation, soil moisture, and climate database, Little River Experimental Watershed, Georgia, United States. *Water Resources Research*, *43*, W09472. https://doi.org/10.1029/2006WR005834.

Bosch, D. D., & Sheridan, J. M. (2007). Stream discharge database, Little River Experimental Watershed, Georgia, United States. *Water Resources Research*, *43*, W09473. https://doi.org/10.1029/2006WR005833.

Bosch, D. D., Sheridan, J. M., Lowrance, R. R., Hubbard, R. K., Strickland, T. C., Feyereisen, G. W., & Sullivan, D. G. (2007). Little River Experimental Watershed database. *Water Resources Research*, *43*, W09470. https://doi.org/10.1029/2006WR005844.

Calvo-Cases, A., Boix-Fayos, C., & Imeson, A. C. (2003). Runoff generation, sediment movement and soil water behaviour on calcareous (limestone) slopes of some Mediterranean environments in southeast Spain. *Geomorphology*, *50*, 269–291. https://doi.org/10.1016/s0169-555x(02)00218-0

Cao, W., Bowden, W. B., Davie, T., & Fenemor, A. (2006). Multi-variable and multi-site calibration and validation of SWAT in a large mountainous catchment with high spatial variability. *Hydrological Processes*, *20*, 1057–1073.

Chescheir, G. M., Gilliam, J. W., Skaggs, R. W., & Broadhead, R. G. (1991). Nutrient and sediment removal in forested wetlands receiving pumped agricultural drainage water. *Wetlands*, *11*, 87–103.

Cho, J., Bosch, D., Vellidis, G., Lowrance, R., & Strickland, T. C. (2012). Multi-site evaluation of hydrology component of SWAT in the coastal plain of southwest Georgia. *Hydrological Processes*, *27*, 1691–1700.

Chow, V. T., Maidment, D. R., & Mays, L. W. (1988). *Applied hydrology*. New York: McGraw Hill.

Dunne, T., & Black, R. D. (1970). Partial area contributions to storm runoff in a small New England watershed. *Water Resources Research*, *6*, 1296–1311.

Eckhardt, K. (2008). A comparison of baseflow indices, which were calculated with seven different baseflow separation methods. *Journal of Hydrology*, *352*, 168–173. https://doi.org/10.1016/j.jhydrol.2008.01.005

Frankenberger, J. R., Brooks, E. S., Walter, M. T., Walter, M. F., & Steenhuis, T. S. (1999). A GIS-based variable source area hydrology model. *Hydrological Processes*, *13*, 805–822. https://doi.org/10.1002/(sici)1099-1085(19990430)13:6<805::aid-hyp754>3.0.co;2-m

Ghebremichael, L. T., Veith, T. L., & Hamlett, J. M. (2013). Integrated watershed- and farm-scale modeling framework for targeting critical source areas while maintaining farm economic viability. *Journal of Environmental Management*, *114*, 381–394. https://doi.org/10.1016/j.jenvman.2012.10.034

Guo, Y. P., Liu, S. G., & Baetz, B. W. (2012). Probabilistic rainfall-runoff transformation considering both infiltration and saturation excess runoff generation processes. *Water Resources Research*, *48*. https://doi.org/10.1029/2011wr011613

Haith, D. A., & Shoemaker, L. L. (1987). Generalized watershed loading functions for stream-flow nutrients. *Water Resources Bulletin*, *23*, 471–478.

Hoffmann, C. C., Kjaergaard, C., Uusi-Kämppä, J., Hansen, H. C. B., & Kronvang, B. (2009). Phosphorus retention in riparian buffers: Review

of their efficiency. *Journal of Environmental Quallity*, *38*, 1942–1955. https://doi.org/10.2134/jeq2008.0087

Kirchner, J. W. (2003). A double paradox in catchment hydrology and geochemistry. *Hydrological Processes*, *17*, 871–874.

Kleinman, P. J. A., Sharpley, A. N., McDowell, R. W., Flaten, D. N., Buda, A. R., Tao, L., … Zhu, Q. (2011). Managing agricultural phosphorus for water quality protection: Principles for progress. *Plant and Soil*, *349*, 169–182. https://doi.org/10.1007/s11104-011-0832-9

Li, H., Sivapalan, M., & Tian, F. (2012). Comparative diagnostic analysis of runoff generation processes in Oklahoma DMIP2 basins: The Blue River and the Illinois River. *Journal of Hydrology*, *418*, 90–109. https://doi.org/10.1016/j.jhydrol.2010.08.005

Lim, K. J., Engel, B. A., Tang, Z., Choi, J., Kim, K., Muthukrishnan, S., & Tripathy, D. (2005). Automated web GIS based hydrograph analysis tool, WHAT. *Journal of the American Water Resources Association*, *41*, 1407–1416.

Lowrance, R. R., Todd, R. L., & Asmussen, L. E. (1983). Waterborne nutrient budgets for the riparian zone of an agricultural watershed. *Agriculture, Ecosystems & Environment*, *10*, 371–384.

Lyon, S. W., McHale, M. R., Walter, M. T., & Steenhuis, T. S. (2006). The impact of runoff generation mechanisms on the location of critical source areas. *Journal of the American Water Resources Association*, *42*, 793–804. https://doi.org/10.1111/j.1752-1688.2006.tb04493.x

Lyon, S. W., Walter, M. T., Gérard-Marchant, P., & Steenhuis, T. S. (2004). Using a topographic index to distribute variable source area runoff predicted with the SCS Curve-Number equation. *Hydrological Processes*, *18*, 2757–2771.

Martinez-Mena, M., Albaladejo, J., & Castillo, V. M. (1998). Factors influencing surface runoff generation in a Mediterranean semi-arid environment: Chicamo watershed, SE Spain. *Hydrological Processes*, *12*, 741–754. https://doi.org/10.1002/(sici)1099-1085(19980430)12:5<741::aid-hyp622>3.0.co;2-f

Melesse, A. M., & Graham, W. D. (2004). Storm runoff prediction based on a spatially distributed travel time method utilizing remote sensing and GIS. *Journal of the American Water Resources Association*, *40*, 863–879. https://doi.org/10.1111/j.1752-1688.2004.tb01051.x

Mishra, S., & Singh, V. (2003). *Soil Conservation Service Curve Number (SCS-CN) methodology*. Netherlands: Springer.

Mishra, S. K., & Singh, V. P. (2004). Long-term hydrological simulation based on the soil conservation service curve number. *Hydrological Processes*, *18*, 1291–1313.

Moriasi, D., Arnold, J., Van Liew, M., Bingner, R., Harmel, R., & Veith, T. (2007). Model evaluation guidelines for systematic quantification of accuracy in watershed simulations. *Transactions of the ASABE*, *50*, 885–900.

Moriasi, D. N., Gitau, M. W., Pai, N., & Daggupati, P. (2015). Hydrologic and water quality models: Performance measures and evaluation criteria. *Transactions of the ASABE*, *58*, 1763–1785.

Muzik, I. (1996). Flood modelling with GIS-derived distributed unit hydrographs. *Hydrological Processes*, *10*, 1401–1409.

Neitsch, S., Arnold, J., Kiniry, J., Williams, J, & King, K. 2011. SWAT2009 theoretical documentation. Texas Water Ressources Institute Technical Report No. 406.

Penna, D., Tromp-van Meerveld, H. J., Gobbi, A., Borga, M., & Dalla Fontana, G. (2011). The influence of soil moisture on threshold runoff generation processes in an alpine headwater catchment. *Hydrology and Earth System Sciences*, *15*, 689–702. https://doi.org/10.5194/hess-15-689-2011

Pionke, H. B., Gburek, W. J., Sharpley, A. N., & Schnabel, R. R. (1996). Flow and nutrient export patterns for an agricultural hill-land watershed. *Water Resources Research*, *32*, 1795–1804.

Rathjens, H., Oppelt, N., Bosch, D. D., Arnold, J. G., & Volk, M. (2015). Development of a grid-based version of the SWAT landscape model. *Hydrological Processes*, *29*, 900–914.

Rawls, W. J., Yates, P., & Asmussen, L. E. (1976). Calibration of selected infiltration equations for the Georgia Coastal Plain. USDA Agricultural Research Service, No. ARS-S-113, 110pp.

Saffarpour, S., Western, A. W., Adams, R., & McDonnell, J. J. (2016). Multiple runoff processes and multiple thresholds control agricultural runoff generation. *Hydrology and Earth System Sciences*, *20*, 4525–4545. https://doi.org/10.5194/hess-20-4525-2016

Seibert, J., & McDonnell, J. J. (2003). The quest for an improved dialog between modeler and experimentalist. In Q. Duan, H. V. Gupta, S. Sorooshian, A. N. Rousseau, & R. Turcotte (Eds.), *Calibration of watershed models* (pp. 301–315). Washington, DC: American Geophysical Union.

Sheridan, J. M. (1997). Rainfall-streamflow relations for coastal plain watersheds. *Applied Engineering in Agriculture*, *13*, 333–344.

Soulis, K., & Dercas, N. (2007). Development of a GIS-based spatially distributed continuous hydrological model and its first application. *Water International*, *32*, 177–192.

Soulis, K., & Dercas, N. (2010). AgroHydroLogos: Development and testing of a spatially distributed agro-hydrological model on the basis of ArcGIS. In: International Congress on Environmental Modelling and Software, Modelling for Environment's Sake, Fifth Biennial Meeting (iEMSs).

Srinivasan, M. S., Gburek, W. J., & Hamlett, J. M. (2002). Dynamics of stormflow generation—A hillslope-scale field study in east-central Pennsylvania, USA. *Hydrological Processes*, *16*, 649–665. https://doi.org/10.1002/hyp.311

Srinivasan, M. S., & McDowell, R. W. (2009). Identifying critical source areas for water quality: 1. Mapping and validating transport areas in three headwater catchments in Otago, New Zealand. *Journal of Hydrology*, *379*, 54–67.

Uusi-Kämppä, J., Braskerud, B., Jansson, H., Syversen, N., & Uusitalo, R. (2000). Buffer zones and constructed wetlands as filters for agricultural phosphorus. *Journal of Environmental Quality*, *29*, 151–158.

How to cite this article: Li S, Gitau M, Bosch D, Engel BA, Zhang L, Du Y. Development of a soil moisture-based distributed hydrologic model for determining hydrologically based critical source areas. *Hydrological Processes*. 2017;31:3543–3557. https://doi.org/10.1002/hyp.11276